

# Major Mergers of Galaxy Haloes: Cuspy or Cored Inner Density Profile?

Michael Boylan–Kolchin<sup>1,2\*</sup> and Chung–Pei Ma<sup>2†</sup>

<sup>1</sup>*Department of Physics, University of California, Berkeley, CA 94720, USA*

<sup>2</sup>*Department of Astronomy, University of California, Berkeley, CA, 94720, USA*

2 November 2018

## ABSTRACT

We present the results from a series of collisionless  $N$ -body simulations of major mergers of galaxy dark matter haloes with density profiles having either inner cusps or cores. Our simulations range from  $2 \times 10^5$  to  $10^7$  particles, allowing us to probe the phase-space distribution of dark matter particles in the innermost regions (less than 0.005 virial radii) of cold dark matter haloes, a subject of much recent debate. We find that a major merger of two cored haloes yields a cored halo and does not result in a cuspy profile seen in many cosmological simulations. This result is unchanged if we consider mergers with parent mass ratios of 3:1 instead of 1:1. Mergers of a cuspy halo with either a cored halo or a second cuspy halo of equal mass, on the other hand, produce cuspy haloes with a slightly reduced inner logarithmic slope. Cuspy haloes, once formed, therefore appear resilient to major mergers. We find the velocity structure of the remnants to be mildly anisotropic, with a Maxwellian velocity distribution near the centre but not in the outer portions of the final haloes. Violent relaxation is effective only during the early phase of mergers, with phase mixing likely to be the dominant relaxation process at late times.

**Key words:** galaxies: haloes – dark matter – methods:  $N$ -body simulations

## 1 INTRODUCTION

In the currently favored cosmological constant plus cold dark matter ( $\Lambda$ CDM) model of cosmology, structure forms hierarchically: small dark matter haloes collapse at high redshifts, while larger and more massive objects form through a series of minor mergers that accrete smaller mass haloes and major mergers with comparable mass haloes. Since dark matter haloes provide the gravitational potential wells necessary for galaxy formation (White & Rees 1978), a detailed understanding of the effects of mergers is necessary in order to test models of galaxy formation and evolution within the  $\Lambda$ CDM paradigm.

Recent numerical studies indicate that the hierarchical build-up process results in haloes with significant substructure populations: hundreds to thousands of subhaloes to the smallest resolvable mass scales appear to reside within galaxy sized haloes, comprising approximately 10% of a halo’s mass (Ghigna et al. 1998; Klypin et al. 1999; Moore et al. 1999b). A number of recent papers have investigated the evolution and detailed properties of the substructure using both semi-analytic models and

numerical simulations. Depending on factors such as the relative mass, pericentric distance, and halo concentration, the orbits and masses of the subhaloes can be strongly affected by dynamical friction and tidal stripping (e.g. Velázquez & White 1999; Taylor & Babul 2001; Hayashi et al. 2003; Taffoni et al. 2003; Benson et al. 2004). Dense subhaloes that survive the tidal process can sink to the centre of the parent halo, impacting its inner structure (e.g. Dekel et al. 2003; Dekel, Devor, & Hetzroni 2003).

In contrast to minor mergers, where large haloes swallow up smaller ones in a relatively gentle fashion, major mergers are more violent events involving systems of approximately equal mass that can be studied in detail with numerical simulations only. The interest in major mergers has a long history. Toomre & Toomre (1972) noted that many observed features of galaxy pairs can be explained by tidal interactions that could promote merging. They further speculated that if such interactions were common enough, elliptical galaxies might naturally be explained as the merger remnants of spiral galaxies. This suggestion has led to numerous studies of galaxy merging and has been quite successful in helping explain the origin of ellipticals. In some of the earliest simulations, White (1978, 1979) studied several types of mergers using 250 simulation particles per halo and concluded that products of mergers of cored galaxies were signif-

\* E-mail: mrbk@astro.berkeley.edu

† E-mail: cpma@astro.berkeley.edu

icantly more centrally concentrated than their progenitors, with more extended haloes having an approximate power-law density profiles  $\rho \propto r^{-3}$  that resembled the de Vaucouleurs’ empirical profile for the surface-brightness of ellipticals (de Vaucouleurs 1948). The higher resolution simulations by Pearce, Thomas, & Couchman (1993) with  $\sim 8000$  particles per halo also exhibited the  $r^{-3}$  behavior with evidence for homology. Simulations with multiple components representing dark matter haloes, stellar disks, and stellar bulges have been a source of much theoretical progress (e.g. Barnes & Hernquist 1992 and references therein) and are essential for elucidating the dynamical coupling between the dark matter and stellar components in galaxies and for comparing simulation results with observations. Pure dark halo simulations, however, are required for a controlled study of the non-baryonic dark matter that dominates the gravitational potential of seemingly all galactic systems.

In this paper we perform high-resolution  $N$ -body simulations of mergers of two equal-mass dark matter haloes and study how the phase-space distribution of dark matter particles is affected by such violent events and how the merger product relaxes into equilibrium. We pay particular attention to the central regions of the haloes and examine whether the initial inner structure of a dark matter halo, either with a flat core or a sharp cusp, is disrupted or preserved by major collisions. Our study complements the numerous recent cosmological  $N$ -body studies of the properties and evolution of dark matter haloes, most of which have reached the somewhat surprising conclusion that over a wide range of mass scales, these haloes are universally cuspy and have radial density profiles with  $\rho(r) \propto r^{-\gamma}$  (with  $1.0 < \gamma < 1.5$ ) in the central region and  $\rho \propto r^{-3}$  near the virial radius (Navarro, Frenk, & White 1997; Fukushige & Makino 1997; Moore et al. 1999a; Ghigna et al. 2000; Fukushige, Kawai, & Makino 2004). The seemingly generic prediction of an inner cusp agrees with earlier simulations (e.g. Dubinski & Carlberg 1991) but is contrary to the inferred dark matter distribution in some dwarf and low surface brightness galaxies (e.g. McGaugh & de Blok 1998; Simon et al. 2003, though also see Swaters et al. 2003) as well as in spiral galaxies (Salucci 2001) and has led to speculation that the  $\Lambda$ CDM model is in crisis.

The simulations of major mergers performed in this paper provide a set of controlled experiments for us to address questions such as: How does the phase space density of dark matter haloes evolve and re-equilibrate during major mergers? Is the cuspy profile an attractor region of the phase space so that merger remnants of two non-cuspy (i.e. cored) haloes will end up cuspy? Do cuspy haloes, once formed (by any process), retain their inner structure after inevitable major mergers with other haloes? Unlike cosmological simulations that are designed to incorporate many complicated processes at once, the simulations performed here allow us to separate out the effects of minor mergers and to focus on how major collisions change the spatial and velocity structures of any initial haloes of our choice. Additionally, cosmological parameters are unimportant for the simulations themselves since major mergers are local processes of two fully collapsed objects. In this case, all we need is the initial phase space distribution of each galaxy halo and the initial relative positions and velocities of the haloes themselves. By

simulating collisions of two galaxy haloes with high spatial resolution and up to 5 million particles (for each halo), we are able to follow their phase-space evolution and the density profiles of the remnants down to  $\sim 0.004 r_{200}$  in our highest resolution simulation.

Section 2 of this paper describes the initial setup and the parameters used in the numerical simulations. We also discuss in some detail the tests performed to quantify the numerical effects of two-body relaxation on the central regions of the haloes and the technical issue of how to determine the centre of a merged halo. Section 3 contains our results from the ten production runs for the energy, density profiles, velocity distributions, and phase space structure of merger remnants. Section 4 discusses the energy distribution and the relaxation of a merged halo to an equilibrium state, with an emphasis on violent relaxation and phase mixing. Section 5 contains a summary of our results.

## 2 PROCEDURE

### 2.1 Initial Conditions

We study two general types of inner density profiles for galaxy haloes: cored and cuspy. For the cored profile, we use an isothermal sphere with a core radius and an exponential cut-off (Hernquist 1993):

$$\rho(r) = \frac{1}{2\pi^{3/2}} \frac{\alpha M}{r_{\text{cut}}} \frac{\exp(-r^2/r_{\text{cut}}^2)}{r^2 + r_{\text{core}}^2} \quad (1)$$

where  $M$  is the halo’s mass,  $\alpha$  is a normalization constant given in terms of  $x \equiv r_{\text{cut}}/r_{\text{core}}$  as  $\alpha^{-1} = 1 - \sqrt{\pi} x e^{x^2} \text{erfc}(x)$ ,  $r_{\text{cut}}$  is the outer exponential fall-off radius and  $r_{\text{core}}$  is the core radius. For the cuspy haloes, we use the Navarro, Frenk, and White (NFW) profile (Navarro, Frenk, & White 1997):

$$\rho(r) = \frac{\rho_c \bar{\delta}}{(r/r_s)(1+r/r_s)^2} \quad (2)$$

with scale radius  $r_s$  and characteristic density  $\bar{\delta}$  given by

$$r_s = \frac{r_{200}}{c} = \frac{1}{c} \left( \frac{3M_{200}}{800\pi\rho_c} \right)^{1/3} \quad (3)$$

$$\bar{\delta} = \frac{200c^3}{3[\ln(1+c) - c/(1+c)]} \quad (4)$$

where  $c$  is the halo concentration parameter and  $r_{200}$  is the radius at which the average interior density is 200 times the critical density of the universe  $\rho_c = 3H^2/8\pi G$ . (We also adopt  $r_{200}$  as a halo’s virial radius and therefore  $M_{200} \equiv 800\pi\rho_c r_{200}^3/3$  as its virial mass.)

We generate our initial conditions using the methods described by Hernquist (1993). The initial positions of the particles in a halo are drawn randomly from its density profile. All of our initial haloes are chosen to be  $10^{12} M_{\odot}$ . In the case of the NFW profile the total mass is formally infinite, so it is necessary to introduce a truncation radius for the halo. We choose to truncate our haloes at  $r = r_{200}$ . For our choice of  $c = 10$ , the virial and truncation radius is  $162.6 h^{-1}$  kpc and the scale radius is  $r_s = r_{200}/c = 16.26 h^{-1}$  kpc. For the cored profile, we choose  $r_{\text{core}} = 8 h^{-1}$  kpc,  $r_{\text{cut}} = 81 h^{-1}$  kpc, and truncate the halo at  $2r_{\text{cut}}$ . This choice of parameters allows us to start with two types of galaxies, equal

in mass and radius, but with very different inner density profiles (core vs. cusp).

For the initial velocities of particles in the frame of a given halo, we first use the Jeans equation (the first moment of the collisionless Boltzmann equation) to relate the density profile  $\rho(r)$  and potential  $\Phi(r)$  to the velocity dispersions (Binney & Tremaine 1987):

$$\frac{d(\rho\sigma_r^2)}{dr} + 2\frac{\beta}{r}\rho\sigma_r^2 = -\rho\frac{d\Phi}{dr}, \quad (5)$$

where the velocity anisotropy is parameterized by

$$\beta = \beta(r) \equiv 1 - \frac{\sigma_\theta^2 + \sigma_\phi^2}{2\sigma_r^2}, \quad (6)$$

and  $\sigma_i^2$  is the dispersion of velocity component  $i$ . If we further assume initial velocity isotropy,  $\beta(r) = 0$ , we can integrate Eqn. (5) to yield the dispersion of the radial velocity as a function of radius,

$$\sigma_r^2(r) = \frac{1}{\rho(r)} \int_r^\infty dR \rho(R) \frac{d\Phi}{dR}. \quad (7)$$

From there, we randomly draw individual velocity components from a Gaussian distribution with variance  $\sigma_r^2(r)$ . Following Hernquist (1993), we impose the additional constraint  $v \leq 0.95v_{\text{esc}}$ , which insures that all particles are initially bound to the halo.

We set up the two colliding haloes to be just touching at the truncation radii initially. The initial relative speed of the two haloes is taken to be the speed one of the haloes would have if the two were in circular orbit about their common centre of mass, i.e.,  $v_{\text{rel}} = 2\sqrt{G\mu/r_{\text{rel}}}$ , where  $\mu$  is the reduced mass and  $r_{\text{rel}}$  is the distance between the halo centres. If the two haloes were point particles, this configuration would give  $v_{\text{rel}} = v_{\text{esc}}/\sqrt{2}$ ; all our simulations are therefore relatively high-speed encounters for bound orbits. In this set-up, and with our choice of halo parameters, the two haloes first cross centres of mass at approximately 1.2 Gyr, then again at 2.2 Gyr. This leaves ample time after the first encounter for the haloes to interact and evolve within the 5.0 Gyr run.

Most of our simulations are head-on collisions with an impact parameter  $b = 0$ . We have also performed two simulations in which the two halo centres are initially offset by  $b = 0.5r_{200}$  in order to test the robustness of our conclusions. In terms of the dimensionless parameter

$$\lambda = \frac{J|E|^{1/2}}{GM^{5/2}} \quad (8)$$

for the total mass  $M$ , energy  $E$ , and orbital angular momentum  $J$ , this corresponds to  $\lambda = 0.042$ . In terms of the parameter  $\epsilon$ , defined as the ratio of the angular momentum to that needed for circular orbit at the same velocity and separation, this set-up yields  $\epsilon = 0.24$ . As a final test of the generality of our findings, we performed two simulations of collisions involving unequal mass haloes with cores.

## 2.2 Simulation Parameters and Numerical Effects

All of our simulations are done using **GADGET**, a publicly available N-body tree code (Springel, Yoshida, & White 2001). **GADGET** is available in serial and massively parallel forms; we have tested both versions on a local linux cluster and the parallel version on the IBM SP2 computers at

**Table 1.** Properties of ten simulations of halo mergers. All simulations involve two  $10^{12}M_\odot$  haloes (except where noted), so  $M_{200} = 2 \times 10^{12}(N_{200}/N_p)M_\odot$

Name	$b^1$ ( $r_{200}$ )	$N_p^2$	$N_{200}^3$	$r(t_r)^4$ ( $h^{-1}$ kpc)
Core1	0	$2 \times 10^5$	$1.58 \times 10^5$	4.035
Core2	0	$2 \times 10^6$	$1.58 \times 10^6$	1.850
Core3	0.5	$2 \times 10^6$	$1.52 \times 10^6$	1.886
Core4 <sup>5</sup>	0	$1.33 \times 10^6$	$1.16 \times 10^6$	1.920
Core5 <sup>5</sup>	0	$1.33 \times 10^6$	$1.09 \times 10^6$	2.025
Cusp1	0	$2 \times 10^5$	$1.34 \times 10^5$	3.595
Cusp2	0	$2 \times 10^6$	$1.35 \times 10^6$	1.436
Cusp3	0	$1 \times 10^7$	$6.72 \times 10^6$	0.765
Cusp4	0.5	$2 \times 10^6$	$1.31 \times 10^6$	1.549
Mixed	0	$2 \times 10^6$	$1.48 \times 10^6$	1.488

<sup>1</sup>impact parameter, in units of  $r_{200}$  for an initial halo

<sup>2</sup>total number of initial particles

<sup>3</sup>total number of particles within virial radius of remnant

<sup>4</sup>radius above which the two-body relaxation time exceeds 5 Gyr

<sup>5</sup>unequal mass ( $M_1 = 3M_2$ ) collision;  $M_1 = 10^{12}M_\odot$

the National Energy Research Scientific Computing Center (NERSC). In these test runs, we use either  $10^5$  or  $10^6$  particles and run for 5.0 Gyr. An important objective of the test runs is to check the level of stability against two-body relaxation for an isolated halo initially in equilibrium. Two-body relaxation is a numerical artifact of running simulations where each simulation particle is on the order of  $10^{60} - 10^{75}$  times more massive than a typical elementary particle dark matter candidate. This leads to significant particle encounters that one does not expect to find in a realistic dark matter halo. As a result, the two-body relaxation timescale effectively puts a limit on the region of the halo that faithfully represents the phase space distribution in the collisionless limit.

Though there has been some disagreement about what regions can be considered reliable beyond the level of two-body relaxation (e.g. Moore et al. 1998; Klypin et al. 2001; Fukushige & Makino 2001; Power et al. 2003; Diemand et al. 2003), a conservative criterion is that the local two-body relaxation timescale  $t_r$ , which we define in terms of the circular velocity  $V_{\text{circ}} = V_{\text{circ}}(r)$ , period  $T(r) = 2\pi r/V_{\text{circ}}$ , and number of particles  $N$  (or equivalently mass  $M$ ) interior to a radius  $r$  as

$$\begin{aligned} t_r(r) &= T(r_{200}) \frac{N}{8 \ln N} \frac{r}{r_{200}} \frac{V_{\text{circ}}}{V_{\text{circ}}(r_{200})} \\ &= \frac{\pi}{4} \frac{N}{\ln N} \sqrt{\frac{r^3}{GM(r)}}, \end{aligned} \quad (9)$$

be at least as large as the age of the universe (Fukushige & Makino 2001; Power et al. 2003). Since our simulations are purely gravitational, with no cosmological expansion, the current age of the universe has no direct meaning for the simulations themselves. As a result, we use the slightly different convergence criterion that the two-body relaxation time be longer than the length of time the simulation has run. We can invert Eqn. 9 to find  $r(t_r)$ , the minimum radius which satisfies  $t_r > t_f$  for the final time of

the simulation  $t_f$ ; we refer to this as our minimum converged radius (see Table 1).

Our test runs of single isolated haloes show that the density profiles are stable at all radii  $r(t_r) < r \lesssim 0.8r_{200}$  for the full 5.0 Gyr of simulation: any change in the profile is under 1%. (Near  $r_{200}$  there are small deviations due to truncating the halo.) Inside  $r(t_r)$ , the behavior is dictated by the structure of the halo. NFW haloes have “temperature inversions” where the maximum velocity dispersion is reached not at the centre but at a finite radius. As a result, two-body relaxation does not cause a contraction of the central regions as is the case with the singular isothermal sphere (the so-called gravothermal catastrophe (Binney & Tremaine 1987)) but rather an expansion as energy is transferred from regions with higher velocity dispersion to lower. Any model with a cusp shallower than  $\gamma = 2$  starts with a temperature inversion (Quinlan 1996) and therefore undergoes an expansion of the central region and a concurrent reduction in central density. The central expansion is then followed by a collapsing stage, initiated once the temperature inversion is eliminated (Quinlan 1996; Hayashi et al. 2003). This process occurs on the evaporation timescale, which is much longer than the length of our simulations at all radii. We do see evolution as a result of two-body interactions well within  $r(t_r)$  for our isolated haloes with  $10^5$  particles, but seems to be minimal even at  $0.5r(t_r)$ . We conclude that our simulations will be converged on all scales greater than  $r(t_r)$  and are likely reliable to even smaller radii.

After obtaining stable isolated haloes, we performed production runs (all using the massively parallelized version of **GADGET**) of halo collisions with different particle numbers to check for convergence in the inner structure of merger remnants. We did production runs with zero impact parameter using  $2 \times 10^5$  and  $2 \times 10^6$  total particles for the core-core collisions, and  $10^7$  particles (in addition to both lower particle number simulations) for an cusp-cusp collision; for a core-cusp collision, we did one run with  $2 \times 10^6$  total particles. For the two runs with non-zero impact parameter, we used  $2 \times 10^6$  total particles. Our two unequal mass mergers were both core-core collisions with mass ratios of 3 : 1. Both runs used the parameters described in Section 2.1 for the more massive galaxy. In one run (core4), we reduced all characteristic radii by a factor of  $3^{1/3}$ , yielding a core radius of 5.55 kpc and a cut-off radius of 55.5 kpc. In the other run (core5), the less massive galaxy had the same length scales as the more massive halo:  $r_{\text{core}} = 8$  kpc and  $r_{\text{cut}} = 81$  kpc, giving a halo that is spatially identical to the heavier one but with the density uniformly lower by a factor of 3. By using these parameters, we can identify how a merging halo having either a smaller core or a lower central density affects the merger process.

For all runs, we use a force softening of  $0.175 h^{-1}$  kpc for our particles, the new cell-opening accuracy parameter (`errTolForceAcc`) of 0.001, and timesteps that are inversely proportional to the acceleration (timestep criterion 1 of **GADGET**). (Our choice of `errTolForceAcc` is somewhat smaller than the maximum allowable value suggested by Power et al. (2003) in their recent thorough investigation of numerical parameters in cosmological simulations, but our tests have shown this value is necessary to obtain results that are independent of machine architecture and whether

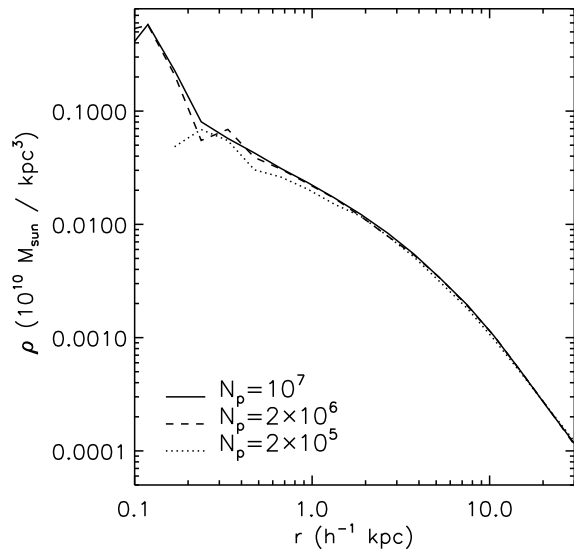


**Figure 1.** Density profiles for 3 different resolution simulations of the merger product of two cuspy haloes at 5 Gyr. The profiles are indistinguishable at large radii, but the profile for the simulation with  $2 \times 10^5$  particles (dotted line) shows signs of numerical relaxation within  $\sim 2 h^{-1}$  kpc.

or not the run is parallel.) A typical run involved between 7000 (core-core runs) and 10000 (cusp-cusp runs) timesteps. Since the crossing time  $t_c = \sqrt{r_{200}^3/GM}$  is approximately 1 Gyr for our haloes, an average timestep corresponds to approximately  $5.9 \times 10^{-4} t_c$ . The parameters for all of the production runs, as well as some results, are summarized in Table 1.

In all of our simulations, at least 65% of the total initial mass ends up within the virial radius of the final halo, meaning there are over  $6 \times 10^6$  particles within  $r_{200}$  in our highest resolution simulation, a large enough number to reliably resolve density contrasts exceeding  $10^6$ . In all runs, at least 97% of the particles stays bound to the final halo. All mergers appear to be mostly completed by 3.5 Gyr, with the virial mass of the haloes increasing by only  $\sim 10\%$  between 3.5 to 5.0 Gyr. Fig. 1 shows the density profiles at the final timestep for the three cusp-cusp collisions. The profiles of the remnants are extremely similar at all radii greater than  $2 h^{-1}$  kpc, and runs “Cusp2” and “Cusp3” have indistinguishable density profiles for radii greater than  $0.7 h^{-1}$  kpc. These results indicate two-body relaxation has not significantly affected any of our haloes at radii larger than  $2 h^{-1}$  kpc and that our two highest resolution cusp-cusp collisions yield density profiles that are reliable on sub-kiloparsec scales.

### 2.3 Definition of Halo Centres

The choice of how to define a halo’s centre is crucial in analyzing the final state of the merger remnant since quantities such as the spherically averaged density profile and radial velocity dispersion depend on the location of the centre. Previous studies have mainly used two methods for defining the centre of a halo: the most bound particle(s) (MBP) and the centre of mass (COM). For example, NFW

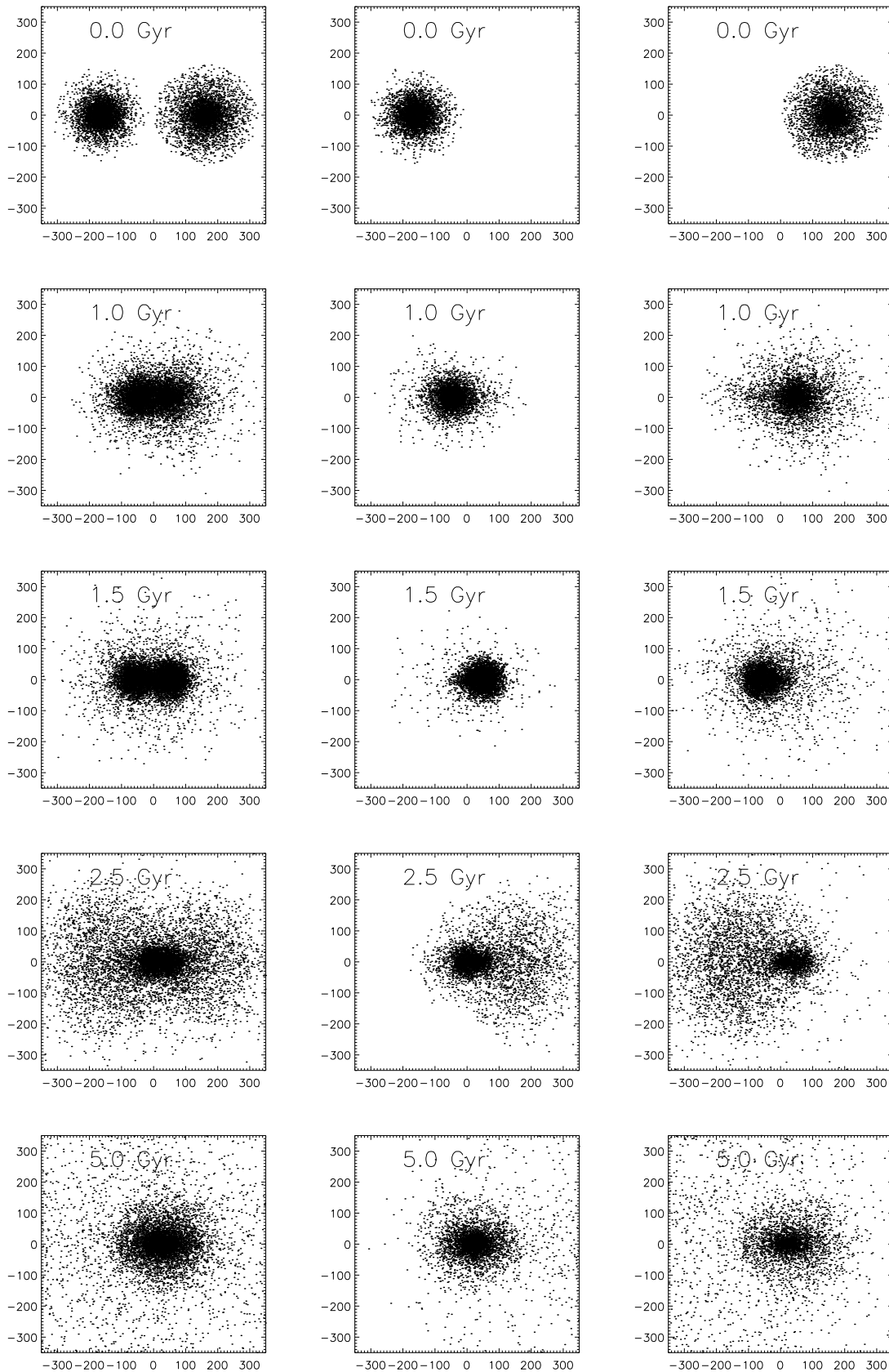


**Figure 2.** Scatter plot of five snapshots for simulation “Mixed” of a cored and a cuspy halo. The collision is along the horizontal axis, and the units of both axes are  $h^{-1}$  kpc. Left: both haloes. Middle: cored halo only. Right: cuspy halo only. The halo centres cross at  $\sim 1.2$  Gyr, then recross at  $\sim 2.2$  Gyr, at which point the relative centre of mass motion is almost completely damped.

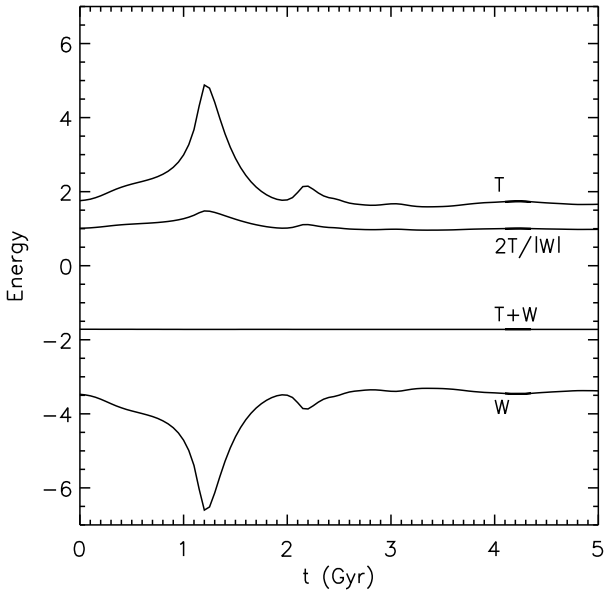


**Figure 3.** Time evolution of the kinetic ( $T$ ), potential ( $W$ ), and total ( $T + W$ ) energies, as well as the virial ratio ( $2T/|W|$ ) for the cusp-core merger simulation. The virial ratio returns to unity soon after the first two encounters at  $\sim 1.2$  and  $2.2$  Gyr. The total energy is conserved to better than 0.4% during the run. The units on the energy axis are arbitrary.

(Navarro, Frenk, & White 1996) use the COM; Moore et al. (1999a) use the MBP and note that it gives very similar results to the COM; Pearce et al. (1993) use the MBP and find that using the COM gives a consistently shallower inner profile.

We adopt an iterative version of the COM technique, which we find to be largely independent of initial assumptions. We have tested this method of computing a halo’s centre against using either the MBP or the COM of the five hundred most bound particles. The resulting spherically averaged density profiles are nearly identical at all radii that we consider to be converged – we find no evidence that one method systematically yields steeper cusps than the other. It is also worth noting that in all cases, the density profiles using different criteria for convergence of the centre of mass calculation differ only at radii that we already consider to be unreliable due to two-body relaxation and Poisson noise. As noted earlier, the density profiles are quite similar over a factor of 50 in particle number (see Fig. 1).

### 3 RESULTS

#### 3.1 Scatter Plots; Energy

Fig. 2 shows five snapshots at  $t = 0, 1, 1.5, 2.5,$  and  $5$  Gyr from the merger simulation of a cored and a cuspy halo (run “Mixed”). (The general sequence of events is the same for all three types of mergers listed in Table 1.) To illustrate the evolution of the individual haloes, we also plot separately the cored halo (middle panels) and cuspy halo (right panels). During the encounter between 1 and 1.5 Gyr, the outer regions of the haloes pass through each other mostly unimpeded; the main effect in the outer portions is for the halo to become more extended. The panels at 2.5 Gyr show that the

**Table 2.** Fits (to Eqn. 11) for three mergers involving cuspy haloes at 5 Gyr.

Name	A ( $10^{10} M_{\odot} \text{kpc}^{-3}$ )	B ( $h^{-1} \text{kpc}$ )	C (cusp slope)
Cusp2	0.00593	9.75	0.672
Cusp3	0.00655	10.0	0.696
Mixed	0.00425	12.1	0.647

cuspy halo’s outer region is more easily stripped away than that of the cored profile; this is as expected, since the NFW profile is more dense in the centre but less tightly bound towards the outer region.

The merger remnants of the head-on collisions are noticeably prolate (extended along the collision axis) with axis ratios of  $\sim 1.6:1:1$  at half-mass radius. This result is quite similar regardless of the initial density profile. The two off-set simulations “Core3” and “Cusp4” with orbital angular momentum result in mildly triaxial remnants.

Fig. 3 shows the evolution of the kinetic, potential and total energies as well as the virial ratio for the same run in Fig. 2. The initial crossing of halo centres is seen to occur at  $\sim 1.2$  Gyr, followed by a second crossing at  $\sim 2.2$  Gyr. Subsequent oscillations are strongly damped, and the system moves towards a steady state in virial equilibrium. The major features in Fig. 3 are common to all production runs listed in Table 1. All runs conserve energy to better than 0.4% and have virial ratios  $2T/|W|$  within 2% of 1.0 by the final timestep.

#### 3.2 Density Profile

In Fig. 4, we plot the spherically-averaged density profiles  $\rho(r)$  of the merger products at 3.5 Gyr (dashed curve) and 5.0 Gyr (solid curve) for each of the three types of collisions: core-core (left), cusp-cusp (middle), and core-cusp (right). The density profiles in all cases are quite stable and constant from 3.5 to 5.0 Gyr, indicating that the merging process is essentially complete by 3.5 Gyr (also evident in Fig. 3) and that our simulations with  $2 \times 10^6$  particles do not suffer much from relaxation effects for the radii shown in Fig. 4. The dotted curves in Fig. 4 show our fitting results to be discussed below. For comparison, we overlay in a separate plot (Fig. 5) the final profiles of the merged haloes at 5 Gyr from the three collisions.

The final product of the core-core collision does *not* show signs of moving towards an NFW profile: the remnant has a core of approximately the same size as in the original haloes. In order to quantify our results, we have tried to fit the final profile to the same functional form as used for the initial cored profile (Eqn. 1). We find the inner region of the remnants well fit by a core radius of  $r_{\text{core}} = 7.8 h^{-1} \text{kpc}$  (for run “Core2”), which is nearly identical to the initial  $r_{\text{core}} = 8 h^{-1} \text{kpc}$ , but the density in the outer region of the remnants falls off more gradually, as  $r^{-3}$  instead of the initial exponential cutoff in Eqn. (1). Overall, we find the merged halo of core-core collisions better fit by

$$\rho(r) = \frac{A}{(r^2 + B^2)^{3/2}}, \quad (10)$$

with  $A \approx 5 \times 10^{10} M_{\odot}$  and  $B \approx 11 h^{-1} \text{kpc}$ , than by the orig-

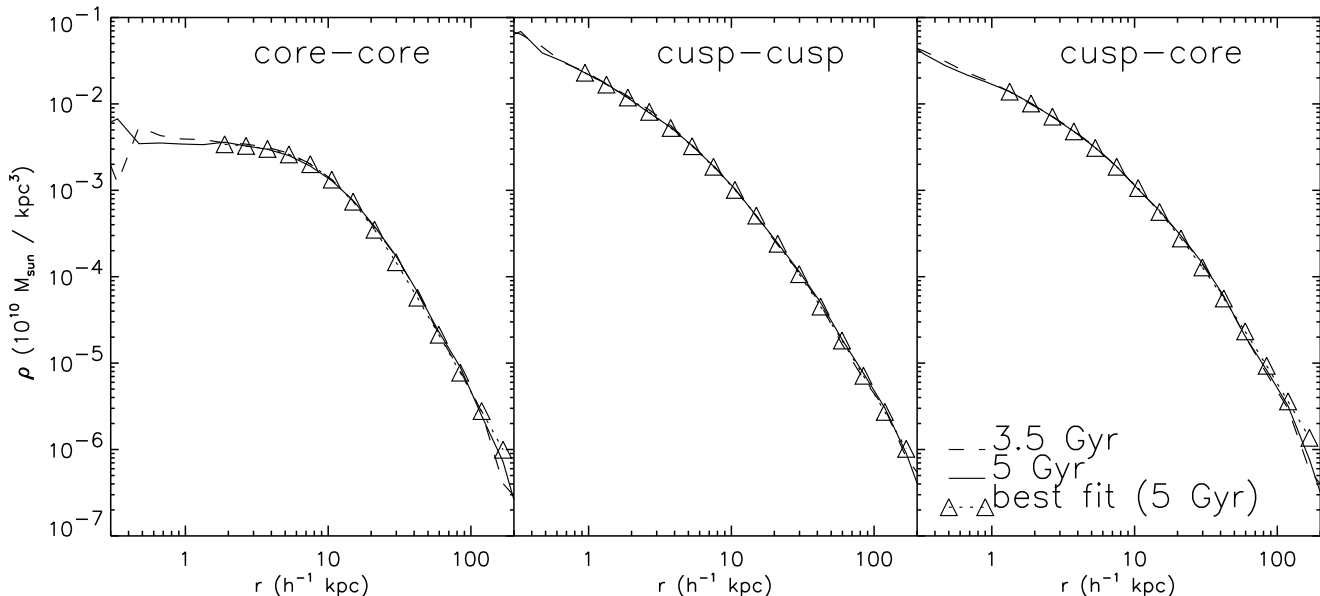


**Figure 4.** Density profiles for the core-core (left), cusp-cusp (centre), and cusp-core (right) simulations with  $2 \times 10^6$  total particles, along with fits from Eqns. 10 and 11. Both the cusp-cusp and the cusp-core collisions are well fit by an NFW-like profile with an inner cusp of  $\gamma \approx 0.7$

inal profile (1). Since the remnants have virial radii about 20% larger than their progenitors, this means the relative size of the core in the final product is smaller, a result consistent with those of earlier simulations (White 1978; Pearce, Thomas, & Couchman 1993). The high spatial and mass resolution used here allows us to simulate scales more than five times below the core radius and to conclude that the core is preserved during one head-on major merger.

In the cusp-cusp collision, the product is essentially a new cuspy halo with an NFW-like form, which we find well fit by

$$\rho(r) = A \frac{B^3}{r^C (B+r)^{3-C}} \quad (11)$$

for radius down to the relaxation scale  $r = 0.7 h^{-1}$  kpc for the  $N_p = 10^7$  particle run. However, the best-fitting value for the logarithmic slope of the cusp is shallower than 1, with  $C \approx 0.7$ , perhaps hinting that collisions of galaxies serve to reduce the cusp at very small radii. The best-fitting parameters for the density profiles of our two highest resolution cusp-cusp collisions, as well as for the core-cusp collision, are summarized in Table 2.

In the case of the core-cusp merger, any hint of the core is entirely eliminated. The remnant has an overall density profile much closer to NFW than to the original core model and again well fit by Eqn. (11) with an inner slope of  $C \approx 0.65$ .

To understand the core-cusp merger in more detail, we calculate the spherically-averaged density profile for particles in each halo separately, first at  $t = 0.0$  Gyr and again at  $t = 5$  Gyr; the results are shown in Fig. 6. Interestingly, the particles originating from the cuspy halo maintain a cuspy, NFW-like profile (left panel), while the particles originating from the cored halo retain their original density profile to a remarkable extent as well (right panel). The final density profile is dominated by the cusp particles in the inner  $\sim 10$  kpc and by the core particles from  $\sim 10 - 100$  kpc; outside

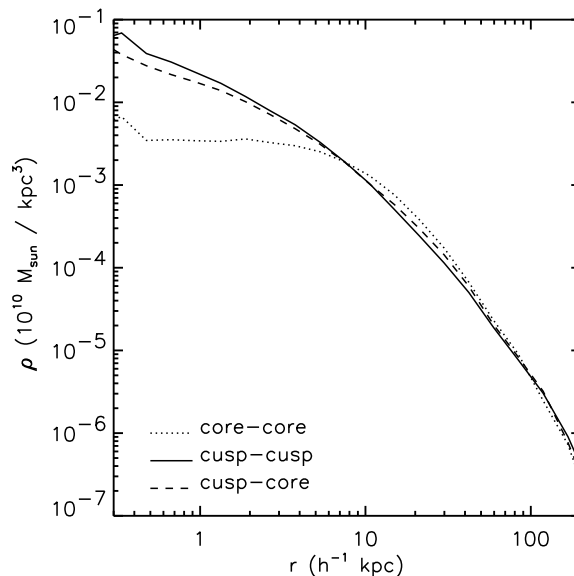


**Figure 5.** Density profiles for the core-core (dotted), cusp-cusp (solid), and cusp-core (dashed) runs with  $2 \times 10^6$  particles at 5.0 Gyr. The cusp-core collision results in a remnant with a density profile much more similar to the cusp-cusp collision than to the core-core one.

of  $\sim 200$  kpc, both types of particles seem to contribute approximately equally (also see Fig. 10).

The results above are all for head-on collisions with a zero impact parameter. In Fig. 7 we compare the density profiles of the non-zero impact parameter runs with the corresponding zero impact parameter simulations. The profiles are almost exactly the same, leading us to the conclusion that introducing moderate amounts of orbital angular momentum into a merging system will not influence our results.

To ensure that the results are not specific to equal-mass

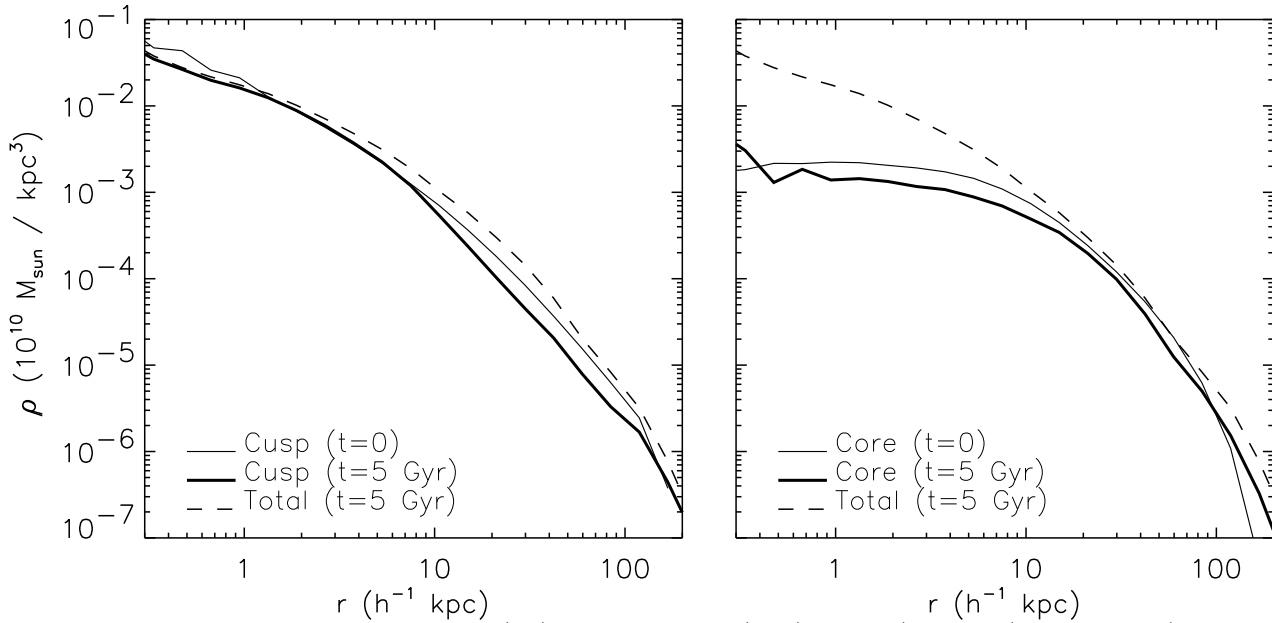


**Figure 6.** Density profiles of the cuspy particles (left) and core particles (right) initially (thin solid) and at 5 Gyr (thick solid) in the core-cusp collision simulation. The particles originating from the cuspy (cored) halo clearly maintain the cuspy (cored) profile after the merger. The dashed line shows the total density profile of the merged halo at 5 Gyr.

mergers, we plot the density profiles of our two 3 : 1 mass mergers in Fig. 8, along with the density profile of the remnant in an equal mass merger for reference. The remnants of both unequal mass mergers retain cores of  $\sim 8$  kpc, the same result we found in the equal mass case. In fact, the final density profiles in all three are remarkably similar; this shows that core-core major mergers produce cored remnants.

### 3.3 Structure of Central Region

Although our simulations are collisionless, resulting in a phase space density that must be conserved due to Liouville’s theorem, we have no *a priori* reason to believe the configuration and momentum space distributions will be independently conserved, i.e. that a merger of two cored (cuspy) haloes will necessarily result in a cored (cuspy) remnant. A system’s coarse-grained distribution function  $\bar{f}$  is constrained to be non-increasing as a function of time (Binney & Tremaine 1987), and thus  $\bar{f}$  in the final state is required at every point to be less than the maximal initial  $\bar{f}$ , but this requirement does not prevent cusps from becoming cores or vice-versa in collisionless simulations. In fact, violent collisions provide strongly fluctuating potentials that cause particles to rapidly exchange energy with the background, a process that could quickly affect the phase space structure of both initial haloes. Since the main objective of our study is to investigate the effects of major mergers on the phase-space distributions of dark matter in the inner regions of galaxy haloes, we examine this region in more detail in this section.

In the core-core and cusp-cusp collisions, we find that as expected, both progenitors contribute essentially equally to the particles at each radius of the merged halo. As Figs. 4 and 5 show, the inner density profile of the merger remnants is similar to their progenitors, i.e., cored haloes remain cored; cuspy haloes remain cuspy.

The situation is more intriguing for the mixed core-cusp

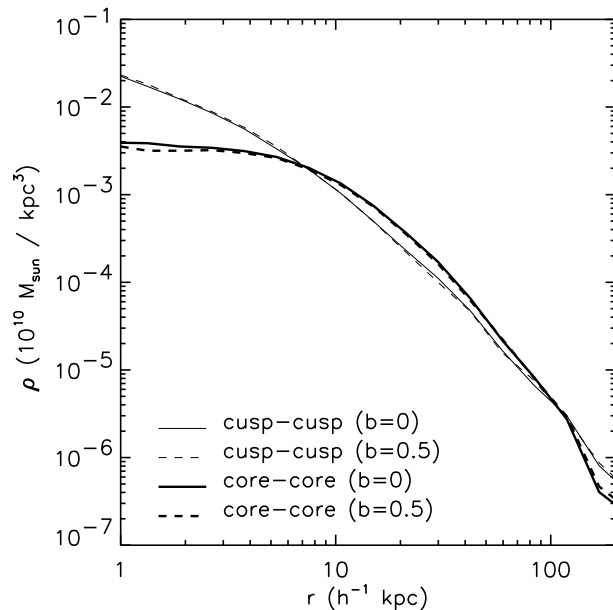


**Figure 7.** Density profiles for cusp-cusp (thin lines) and core-core (thick lines) runs with  $N_p = 2 \times 10^6$  for  $b = 0$  (solid) and  $b = 0.5r_{200}$  (dashed) at 3.5 Gyr. The profiles are extremely similar, indicating that introducing a moderate amount of orbital angular momentum does not significantly impact the merger remnant.

collision. In order to elucidate the inner structure of this type of mergers, we first examine where the initial inner particles in each halo end up in the merged halo after 5 Gyr. (The results at 3.5 Gyr are very similar.) Fig. 9 shows the fraction of particles in each halo that start out within radius  $r$  initially and also remain within  $r$  at 5 Gyr. (By construction, this fraction approaches 1 at large  $r$ .) It shows that in the innermost several kiloparsecs of the merged halo, about 60% of the cusp particles (solid curve) that originated



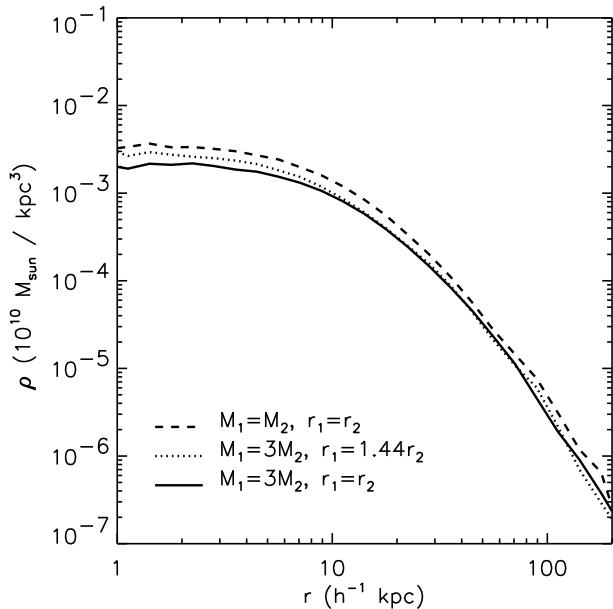


**Figure 8.** Density profiles for three different core-core mergers at 3.0 Gyr. Dashed line: run Core2 (equal mass, both core radii = 8 kpc). Dotted line: run Core4 ( $M_1 = 3M_2$  with core radii  $r_1 = 8$  kpc,  $r_2 = 5.55$  kpc). Dashed line: run Core5 ( $M_1 = 3M_2$  with core radii  $r_1 = r_2 = 8$  kpc). All three mergers produce similar remnants with cores that are unreduced relative to the larger of the two initial cores, showing that mergers of cored haloes result in cored remnants.

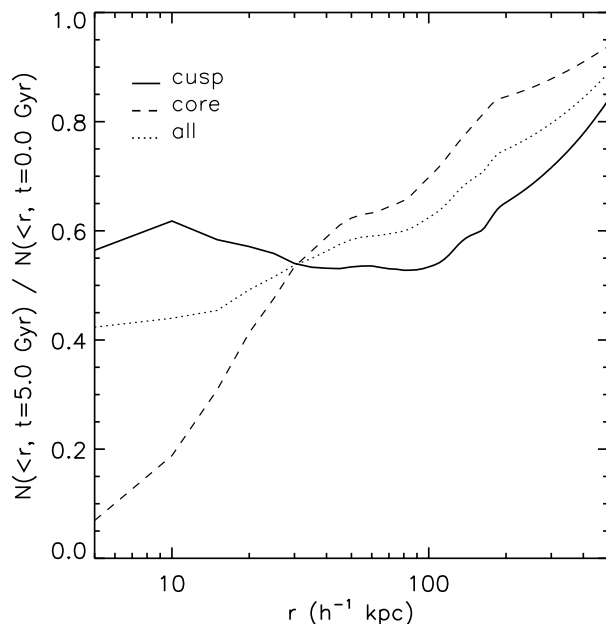


**Figure 9.** Fraction of particles starting out within radius  $r$  at  $t=0$  Gyr that also end up within radius  $r$  at  $t=5$  Gyr (from run Mixed). The cuspy particles (solid line) are much more likely to stay within the inner 10 kpc than the cored particles (dashed line).

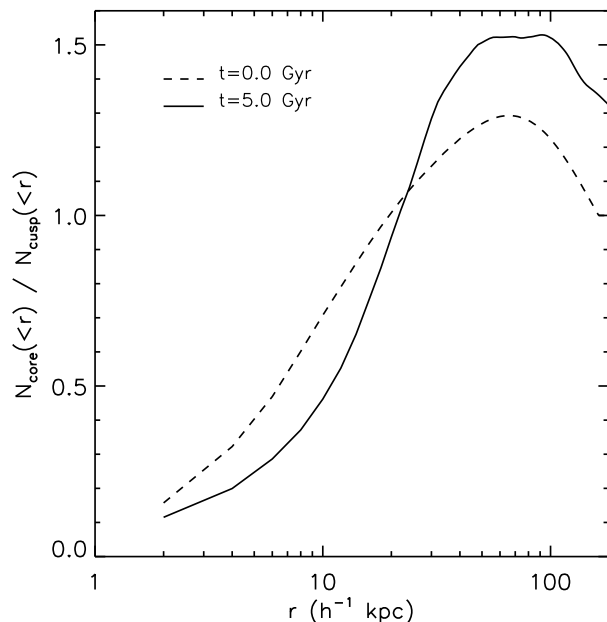


**Figure 10.** Ratio of the number of core particles within radius  $r$  to number of cusp particles within radius  $r$  for the cusp-core collision at  $t=0$  Gyr (dashed) and  $t=5$  Gyr (solid). The remnant is even more centrally dominated by cusp particles than would be the case if the two initial haloes were superimposed, further showing how the core particles dominate the inner structure of the remnant.

from within a given radius stay within that same radius, while very few of the core particles (dashed curve) remain. We believe it is this “lack of mobility” of the cusp particles that gives the cuspy halo a stronger influence at the final remnant’s centre and forces the final density profile to be cuspy rather than cored.

Next we examine the relative contribution of cusp vs core particles to the total density (or potential) in the core-cusp collision. Fig. 10 shows the ratio of core to cusp particles initially (dashed curve) and at 5.0 Gyr (solid curve). The figure shows that the cusp particles dominate the core particles number-wise in the centre initially (if the two galaxies were superimposed with a common centre), and that at 5 Gyr, the central region of the merger remnant becomes even more dominated by cusp particles. This result implies that the tightly bound particles in a cusp tend to stay bound together, while a core is much easier to disrupt. This complements the information from Fig. 9 by showing that for all particles of a given type, regardless of origin, the cuspy particles tend to take over the central region. Moving outward, the core particles begin to contribute more to the remnant. Note that the radius where the number of core particles is equal to the number of cusp particles stays almost constant at  $r \approx 20h^{-1}$  kpc. This is one indication that there is not a major reconfiguration of the particles occurring during the course of the simulation. We have also calculated the quantities in Figs. 9 and 10 at 3.5 Gyr and find them to be very similar to those found at 5 Gyr. This corroborates the evidence in Fig. 3 that the merger is essentially completed by 3.5 Gyr.

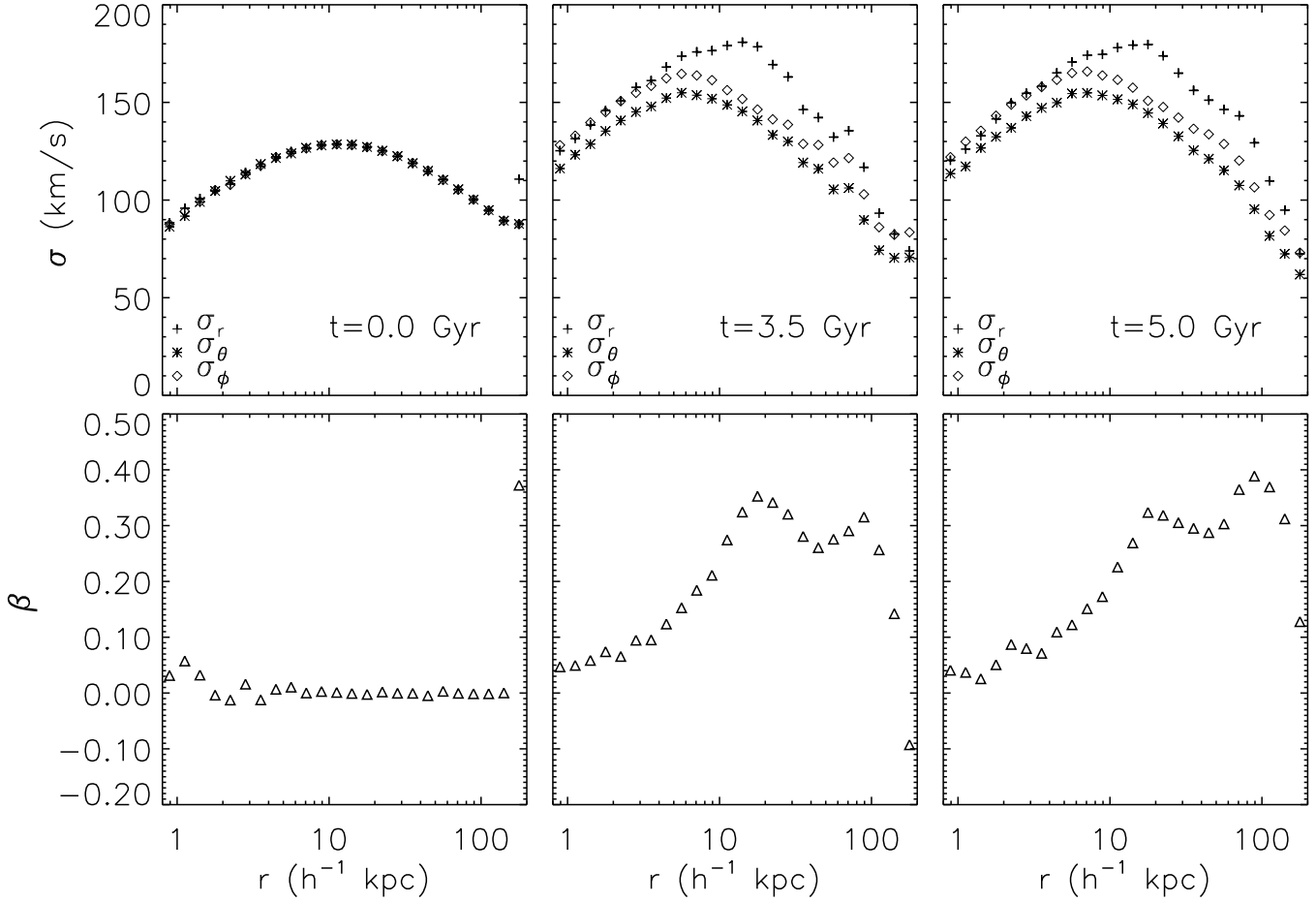


**Figure 11.** Velocity dispersions  $\sigma_r$ ,  $\sigma_\theta$ ,  $\sigma_\phi$  (top) and velocity anisotropies (bottom),  $\beta \equiv 1 - (\sigma_\theta^2 + \sigma_\phi^2)/2\sigma_r^2$ , as a function of halo radius  $r$  from the cusp-cusp merger run with  $10^7$  particles (run “Cusp3”). Three time outputs are shown: 0 Gyr (left), 3.5 Gyr (middle), and 5 Gyr (right). All three velocity dispersions increase after the collision, and the initially isotropic state becomes somewhat anisotropic outside the central region.

### 3.4 Velocity Profile

The particle velocities in our initial haloes are isotropic by construction, but those in our final haloes all exhibit some degree of anisotropy. For the cusp-cusp collision, Fig. 11 shows the velocity dispersions (top panels) and velocity anisotropy (bottom panels) as a function of halo radius  $r$  at  $t = 0, 3.5,$  and  $5$  Gyr for the simulation with  $10^7$  particles (run “Cusp3” in Table 1). The velocities remain mostly isotropic (i.e.  $\beta = 0$ ) near the centre of the merger remnant, but become mildly anisotropic ( $\beta < 0.40$ ) with increasing radius due to radial infalls.

We have also examined the velocity distribution function for the same cusp-cusp run. We find that in the central region of the merged haloes, the velocities are quite Gaussian in addition to being isotropic; Fig. 12 shows  $f(v_i)$  vs.  $v_i$  for  $i = r, \theta, \phi$  for  $10^4$  particles in a radial bin arbitrarily centred on  $10.106$  kpc. The distribution function of  $v_r$  (left panel) is well fit by a Gaussian (dashed line) with width  $\sigma_r = 177 \text{ km s}^{-1}$ , computed from the particles in that bin. The distributions of  $v_\theta$  (middle panel) and  $v_\phi$  (right panel) are also reasonably well fit by the corresponding Gaussians:  $\sigma_\theta = 153 \text{ km s}^{-1}$  and  $\sigma_\phi = 161 \text{ km s}^{-1}$ . Moving away from

the centre, we find the radial distribution becomes substantially less Gaussian and the angular distributions remain mostly Gaussian in the intermediate portion of the halo. Near the virial radius, however, none of the distributions are Gaussian.

The core-core collision exhibits similar trends as in Figs. 11 and 12, so we will not show the results here.

For the core-cusp collision, we plot in Fig. 13 the radial velocity dispersion  $\sigma_r$  as a function of radius  $r$  at  $t = 0, 2.5,$  and  $3.5$  Gyr for the core (crosses) and cusp (diamonds) particles separately. (Little evolution occurs after 3.5 Gyr.) The dispersion of the particles in the cuspy halo changes moderately between 0.0 and 3.5 Gyr, with the peak in  $\sigma_r$  rising and moving outward but the overall shape maintained. For the particles in the cored halo, however, the velocity dispersion near the centre has almost doubled to  $\sigma_r \approx 230 \text{ km s}^{-1}$  after the merger.

To understand why the velocity dispersion of the core particles increases toward the centre of the merged halo upon merging with a cuspy halo, it is instructive to consider a situation where the two haloes are spherically symmetric and share a common centre. In this case, the potential  $\Phi$  is

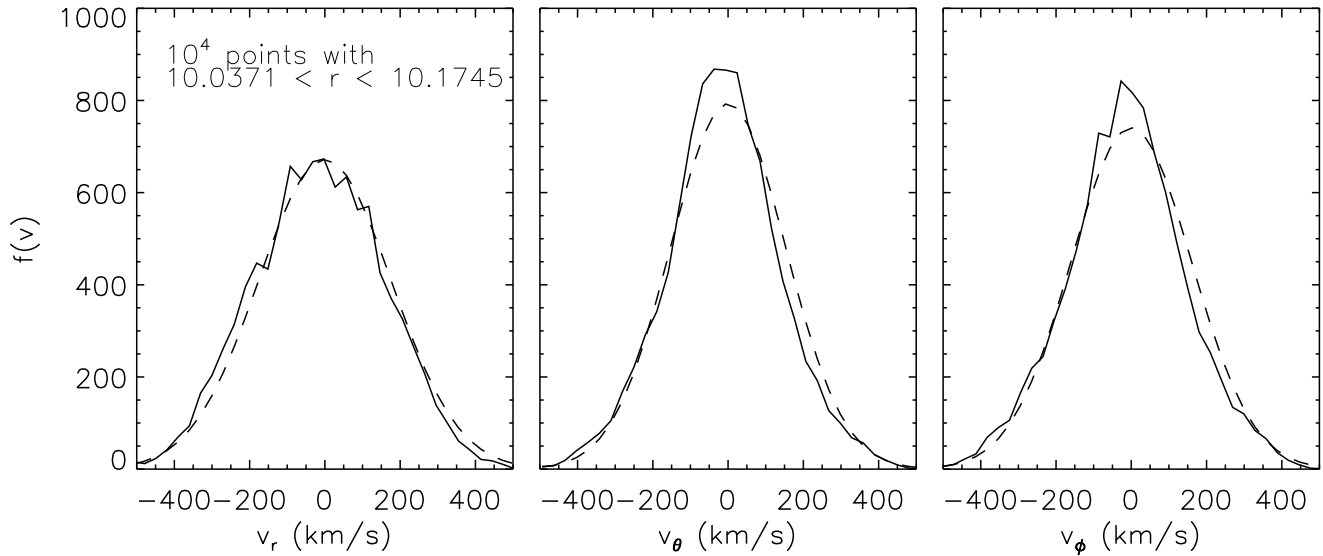


**Figure 12.** Velocity distribution functions (solid) for  $v_r$  (left),  $v_\theta$  (middle), and  $v_\phi$  (right) for  $10^4$  particles in radial bin  $10.0371 < r < 10.1745$  kpc from the cusp-cusp run with a total of  $10^7$  particles at 5 Gyr. The distributions are well-fit by Gaussians (dashed) with width  $(\sigma_r, \sigma_\theta, \sigma_\phi) = (177, 153, 161)$  km s $^{-1}$  calculated from the particle velocities.

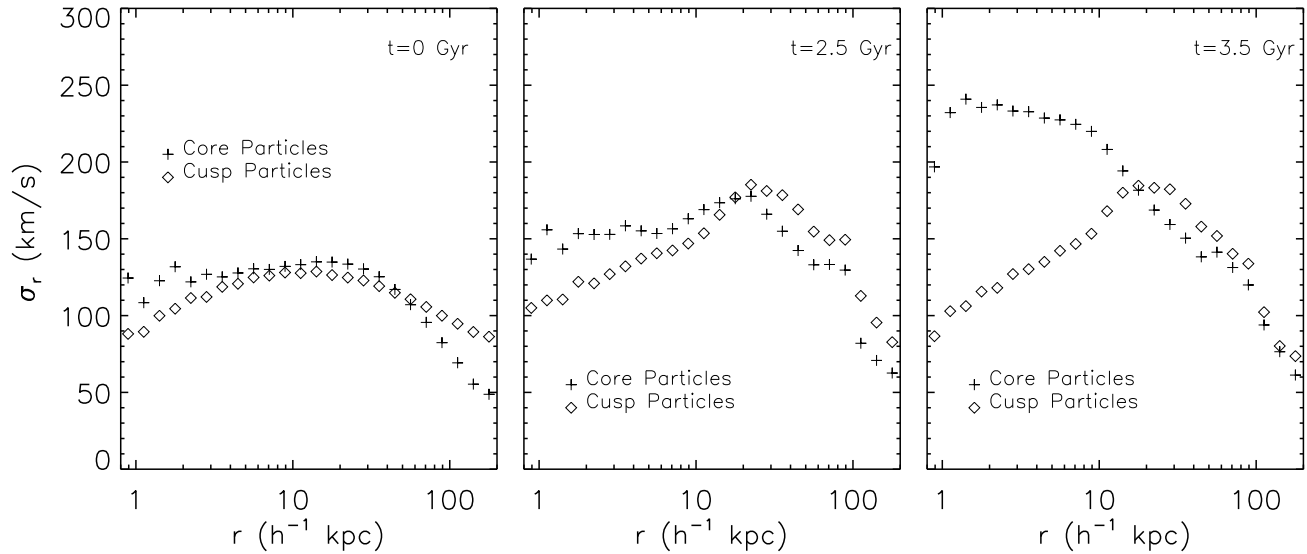


**Figure 13.** Radial velocity dispersion  $\sigma_r$  as a function of halo radius  $r$  from the core-cusp merger run. Three time outputs are shown: 0 Gyr (left), 2.5 Gyr (middle), and 3.5 Gyr (right). Particles originating from the cored (crosses) and cuspy haloes (diamonds) are shown separately. These two types of particles have comparable  $\sigma_r$  initially, but the core particles end up with significantly higher  $\sigma_r$  in the inner 10 kpc than the cusp particles after the merger. The cusp particles are also heated, especially at  $r \sim 10 - 30 h^{-1}$  kpc, as a result of the merger.

a function of the radial coordinate only and can be written as  $\Phi(r) = \Phi_1(r) + \Phi_2(r)$ , a sum of the individual potentials  $\Phi_1(r) = \Phi_{\text{core}}$  and  $\Phi_2(r) = \Phi_{\text{cusp}}$ . For particles in either the cored or cuspy halo, we then have

$$\begin{aligned} \sigma_r^2(r) &= \frac{1}{\rho(r)} \int_r^\infty dR \rho(R) \left( \frac{d\Phi_1}{dR} + \frac{d\Phi_2}{dR} \right) \\ &= \frac{1}{\rho(r)} \int_r^\infty dR \frac{G\rho(R)}{R^2} M_{\text{tot}}(R), \end{aligned} \quad (12)$$

where  $M_{\text{tot}}(R) = M_1(R) + M_2(R)$  is the total mass interior

to radius  $R$ . From the point of view of the core particles, adding the cuspy particles has the effect of adding considerable extra mass and thus deepening the potential.

If the density profile of the core particles remains roughly constant, then adding extra mass in the form of cuspy particles essentially heats the core particles to higher a velocity dispersion, as seen in Fig. 13. The reverse is also true: the core particles also heat the cusp particles. This effect is actually seen in Fig. 13, as the cuspy particles' dispersion increases relative to the original value, especially

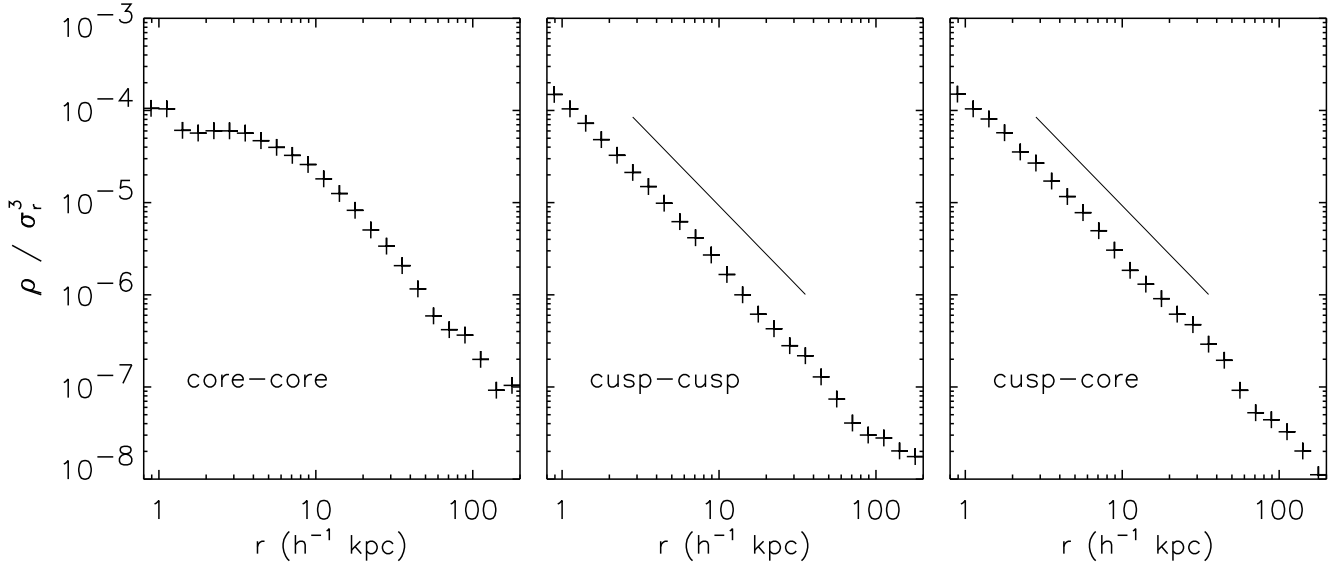


**Figure 14.** Local phase space density, defined as  $F = \rho(r)/\sigma^3(r)$ , for the  $N_p = 2 \times 10^6$  simulations of core-core (left), cusp-cusp (centre), and cusp-core (right) mergers. The densities are normalized to be equal to that of the cusp-cusp simulation at  $r = 1 \text{ h}^{-1} \text{ kpc}$ . The cusp-cusp and cusp-core collisions give phase space densities that can be approximated by a single power law,  $F \propto r^{-1.75}$  (overplotted line), for  $r \leq r_{200}$  while the core-core collision cannot.

noticeably near the original peak of  $\sim 10 \text{ h}^{-1} \text{ kpc}$ . Since the cuspy particles dominate the total mass at radii less than this, however, the core particles are a small perturbation and do not change the cuspy particles' dispersion significantly. The change in the peak of the NFW particles' dispersion from  $\sim 10$  to  $\sim 30 \text{ h}^{-1} \text{ kpc}$  can also be understood in this manner, since the core particles actually contribute more of the interior mass at this radius, as shown in Fig. 10.

### 3.5 Phase Space Profiles

The previous subsections discussed the density and velocity profiles separately. It is also instructive to examine the local phase space density  $\rho(r)/\sigma^3(r)$ , which is shown in Fig. 14 for the three types of mergers studied in this paper. We find that for both the cusp-cusp (middle panel) and core-cusp (right panel) mergers, although the individual  $\rho(r)$  and  $\sigma(r)$  are not a pure power-law in  $r$  (see Figs. 4, 11, and 13), the ratio is interestingly well-approximated by a power law  $\rho/\sigma^3 \propto r^{-\alpha}$ , where the best-fitting slope is  $\alpha \approx 1.75$  for both mergers. The core-core merger (left panel), on the other hand, shows a core in the phase space density since both  $\rho(r)$  and  $\sigma(r)$  are constant at  $r < r_{\text{core}}$ .

Our power-law results can be compared with Taylor & Navarro (2001), who have suggested that the phase space structure of haloes is intimately related to that of self-similar collapse onto spherical density perturbations in an expanding universe. They solved the Jeans equation under the assumption of isotropy and power-law  $\rho/\sigma^3 \propto r^{-\alpha}$  and found that haloes with the NFW profile are well-approximated by the same power law,  $\alpha = 1.875$ , as the self-similar solutions in secondary spherical infall models (Bertschinger 1985; Fillmore & Goldreich 1984; Gott 1975; Gunn 1977). Since the phase space density is inversely proportional to the local entropy, Taylor & Navarro were led to the conclusion that CDM halo structure may be driven

toward the most sharply peaked phase space distribution allowable for a monotonically decreasing density profile. For a power law phase space density, this solution yields density profiles that are very similar to the NFW profile but with a slightly shallower inner cusp,  $\rho \propto r^{-0.75}$  rather than  $r^{-1}$ .

Using the power-law result  $\rho/\sigma^3 \propto r^{-1.75}$  in Fig. 14, we obtain from the Jeans equation a density profile  $\rho \propto r^{-0.72}$ , which is consistent with the best-fitting inner slope shown in Sec. 3.2. One can also look at the question in reverse, i.e., given a power-law density  $\rho \propto r^{-\gamma}$ , what solutions are admitted for the phase space density? Calculations show that  $\gamma \approx 0.7$  cusps lead to phase space densities well approximated by  $\rho/\sigma^3 \propto r^{-1.75}$  as  $r \rightarrow 0$ , but the slope of  $\rho/\sigma^3$  is not strictly a constant beyond the central region (Singh & Ma, in preparation).

## 4 DISCUSSION

Our simulations offer insight into the mechanisms that drive a merging system toward an equilibrium structure, e.g., violent relaxation (Lynden-Bell 1967) and phase mixing. Violent relaxation is due to a time-varying potential which allows the non-conservation of individual particles' energies. The relative motion of the two haloes at the start of our simulations provides such a fluctuating potential. From Fig. 3, it is clear our mergers involve a rapid transfer of orbital energy to internal energy of the individual haloes (and subsequently the merger remnants). The decay of orbital motion occurs approximately on the crossing timescale, with essentially all energy in the form of the remnants' internal energy by 2.5 Gyr. That the orbital motion is so heavily damped and that the remnant haloes do not expand or collapse significantly indicate that the time-varying potential necessary for violent relaxation is eliminated relatively quickly. One possible exception is that density waves could enable violent relaxation

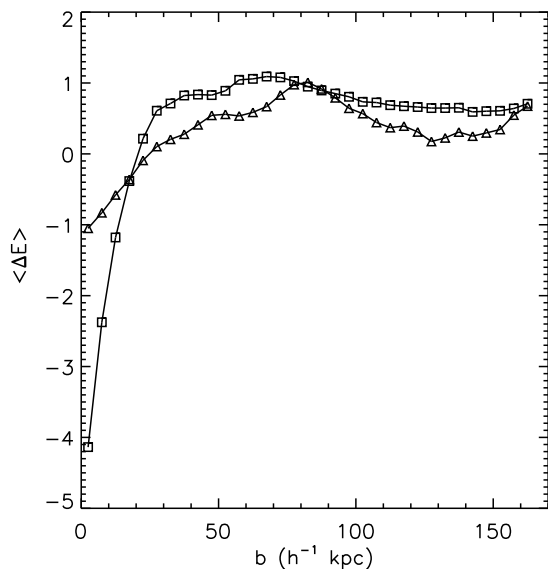


**Figure 15.** Average energy change (in arbitrary units) versus impact parameter for the cusp-core collision. Squares are particles from the cuspy halo, triangles are particles from the cored halo. All particles with small impact parameters tend to lose energy, while those with large impact parameters gain energy. The effect is more dramatic for cuspy particles than cored ones.

to persist even once the haloes have merged. Phase mixing tends to damp these waves strongly, however, with a decay timescale of  $\tau \approx \lambda/\sigma$  for a perturbation of size  $\lambda$ . Taking  $\sigma_r = 150 \text{ km s}^{-1}$  to be typical for our merged haloes, this means that phase mixing will damp out all perturbations smaller than the virial radius within  $\sim 1$  Gyr of the haloes merging. In our simulations, this seemingly short timescale for violent relaxation is sufficient to drive the velocity distribution function in the inner region of the merged halo to a Gaussian form, as predicted by statistical reasoning (e.g. Nakamura 2000). That the distribution function becomes less Gaussian with increasing radius is also in line with expectations because much less mixing is possible in the outer regions of the halo on the timescales we are studying.

Following the energy distribution through the collision can help in understanding the structure of the final product. A particularly interesting quantity is the change in energy  $\Delta E$  for a particle from initial to final state as a function of position. Funato, Makino, & Ebisuzaki (1992) describe an energy segregation in their collision simulations: particles with higher (less negative) energy tend to gain more energy than particles with lower energy. This means a particle near the centre of an initial halo should, on average, lose energy (i.e. become more tightly bound) relative to a particle near the virial radius of a halo. We follow the energy change of each particle, and plot in Fig. 15 the change in energy as a function of impact parameter for the core-cusp run “Mixed”. As Funato et al. describe, the particles with small impact parameters tend to lose energy, while the particles with large impact parameters tend to gain it. The effect is more dramatic for the cuspy particles than for the core particles, perhaps because the inner portion of the cuspy halo is initially more tightly bound but with an essentially equal velocity dispersion profile. As noted by Merril & Henriksen

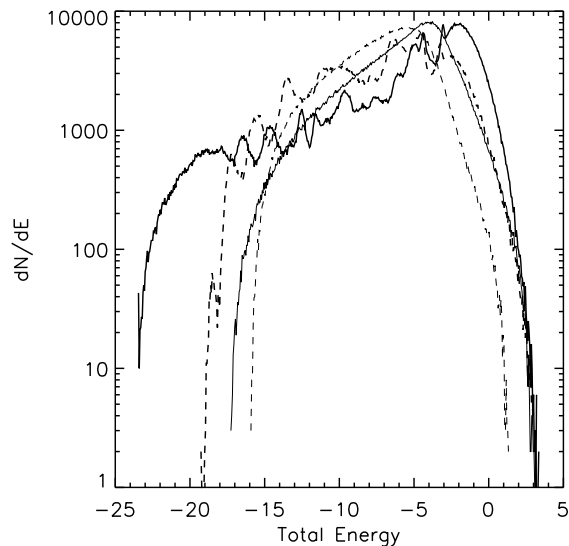


**Figure 16.** Differential energy distribution for the cusp-core merger. the solid lines show the cusp particles and the dashed lines show the core particles; thin lines indicate the initial distributions and thick lines the final distributions. Both distributions are broadened as a result of the merger, and shell-like structures are visible in the final distributions. The energy units are arbitrary.

(2003), however, this energy segregation does not prevent the system from equilibrating via violent relaxation, at least in the central region.

Another interesting quantity is the differential energy distribution  $dN/dE$ , which can be written as a product of the phase-space distribution function  $f(E)$  and the density of states  $g(E)$  (Binney & Tremaine 1987):

$$\frac{dN}{dE} = f(E)g(E). \quad (13)$$

The shape of  $dN/dE$  is therefore *not* the same as the shape of  $f(E)$ . In Fig. 16 we plot  $dN/dE$  for the core-cusp merger, for both types of particle, at the start of the simulation (thin curves) and at 5 Gyr (thick curves). It shows that  $dN/dE$  is broadened, a natural outcome of mergers where the range of energies accessible to an individual particle can change drastically. The wave-like features in  $dN/dE$  at 5 Gyr are indications of shells of particles formed via phase-mixing (Spergel & Hernquist 1992). We note that unlike  $f(E)$ , which generally decreases with increasing  $E$ , the shape of  $dN/dE$  is skewed towards higher energies because of the density of states. Both  $f(E)$  and  $dN/dE$  have been studied analytically for isolated NFW (Widrow 2000) and King haloes (Binney & Tremaine 1987) in equilibrium. The overall shape of  $dN/dE$  resembles that shown in Fig. 16.

## 5 SUMMARY

We have simulated major mergers of galaxy haloes with both cuspy and cored inner density profiles using GADGET, a versatile N-body tree code. Our findings can be summarized as follows:

- (i) Mergers of two cored haloes of equal mass result in

a cored halo. The core radius of the merged halo is nearly identical to those of the original haloes, but the core to virial radius ratio is reduced, with the outer density profile of the merger remnant well approximately by  $\rho \propto r^{-3}$ . This result also holds for mergers with parent halo mass ratios of 3:1, implying all major mergers of two cored haloes result in cored haloes.

(ii) Mergers of a cuspy halo with either a cored halo or a second cuspy halo result in a cuspy halo. If the cuspy halo starts out with an NFW form, the merged halo also has an NFW-like form, with a slightly shallower inner cusp of  $\rho \propto r^{-0.7}$  instead of  $r^{-1}$ .

(iii) The particles from a given halo retain memory of their progenitor’s density profile. In major mergers of a cored halo with a cuspy halo, the particles originating from the cuspy halo end up with a cuspy profile, and those from the cored halo end up with a cored profile. (The cuspy particles dominate the total potential at the centre of the merged halo, so the resulting profile is cuspy.) The core particles in the inner  $10 h^{-1}$  kpc of the remnant are significantly heated.

(iv) The merger remnants relax from the inside outwards, attaining Gaussian velocity distributions near their centres but not throughout the halo. Violent relaxation due to time-varying potential is effective only during the initial phase of the mergers; phase mixing is likely the dominant relaxation process at late times.

(v) Including a moderate amount of orbital angular momentum in the form of a non-zero impact parameter has little discernible effect on our findings.

The set of simulations presented in this paper has been performed for mergers of non-spinning haloes in a set bound orbit. This clearly only probes a restricted range of parameter space. A possible area for future investigations is to include non-zero initial spins, which can influence tidal interactions significantly but may only affect the final phase space structure weakly (White 1979). We have also chosen not to convolute the issues in this paper by ignoring minor mergers with satellite haloes and continuous accretion of diffuse material. The latter mechanisms may be responsible for generating the first generation of cuspy haloes from initially cored haloes, a process not achieved by major mergers of cored haloes according to our study.

Although the length and time scales quoted in this paper are for Milky-Way sized haloes of  $10^{12} M_{\odot}$ , there is nothing in the numerical code or in our analysis that is special to this particular mass scale (except a mildly mass-dependent concentration parameter for NFW haloes). Our conclusions in this paper are thus likely to be applicable to major mergers of comparable-mass haloes over a wide mass range. Our finding that cuspy haloes are resilient to major mergers hints that the existence of cuspy haloes is natural in the hierarchical structure formation scenario: the build-up to larger mass haloes via repeated merging may be sufficient to produce cuspy haloes from cored haloes and preserve the general structure of cuspy haloes.

## ACKNOWLEDGMENTS

We thank Jon Arons, Andrew Benson, Andrey Kravtsov, and Volker Springel for useful discussions and Jeff Filipini for help with the energy analysis. This research used

resources of the National Energy Research Scientific Computing Center, which is supported by the Office of Science of the U.S. Department of Energy under Contract No. DE-AC03-76SF00098. C.-P. M is partially supported by an Alfred P. Sloan Fellowship, a Cottrell Scholars Award from the Research Corporation, and NASA grant NAG5-12173.

## REFERENCES

- Barnes, J. E., Hernquist, L. 1992, *ARA&A*, 30, 705  
 Benson, A. J., Lacey C. G., Frenk C. S., Baugh C. M., Cole S. 2004, *MNRAS*, submitted (astro-ph/0307298)  
 Bertschinger E. 1985, *ApJS*, 58, 39  
 Binney J., Tremaine S. 1987, *Galactic Dynamics*, Princeton University Press, Princeton, N. J.  
 de Vaucouleurs G. 1948, *Ann. d’Astrophys.*, 11, 247  
 Dekel A., Arad I., Devor J., Birnboim Y. 2003, *ApJ*, 588, 680  
 Dekel A., Devor J., Hetzroni G. 2003, *MNRAS*, 341, 326  
 Diemand J., Moore B., Stadel J., Kazantzidis S. 2003, submitted to *MNRAS*, astro-ph/0304549  
 Dubinski J., Carlberg R. G. 1991, *ApJ*, 378, 496  
 Fillmore J. A., Goldreich P. 1984, *ApJ*, 281, 1  
 Fukushige T., Makino J. 1997, *ApJ*, 477, L9  
 Fukushige T., Makino J. 2001, *ApJ*, 557, 533  
 Fukushige T., Kawai M., Makino J. 2004, *ApJ*, submitted (astro-ph/0306203)  
 Funato Y., Makino J., Ebisuzaki T. 1992, *PASJ*, 44, 291  
 Ghigna S., Moore B., Governato F., Lake G., Quinn T., Stadel J. 1998, *MNRAS*, 300, 146  
 Ghigna S., Moore B., Governato F., Lake G., Quinn T., Stadel J. 2000, *ApJ*, 544, 616  
 Gott J. R. 1975, *ApJ*, 201, 296  
 Gunn J. E. 1977, *ApJ*, 218, 592  
 Hayashi E., Navarro J. F., Taylor J. E., Stadel J., Quinn T. 2003, *ApJ*, 584, 541  
 Hernquist L. 1993, *ApJS*, 86, 389  
 Klypin A., Kravtsov A. V., Valenzuela O., Prada F. 1999, *ApJ*, 522, 82  
 Klypin A., Kravtsov A. V., Bullock J. S., Primack J. R. 2001, *ApJ*, 554, 903  
 Lynden-Bell D. 1967, *MNRAS*, 136, 101  
 McGaugh S. S., de Blok W. J. G. 1998, *ApJ*, 499, 41  
 Merril T., Henriksen R. 2003, *ApJ*, 595, 43  
 Moore B., Governato F., Quinn T., Stadel J., Lake G. 1998, *ApJ*, 488, L5  
 Moore B., Quinn T., Governato F., Stadel J., Lake G. 1999a, *MNRAS*, 310, 1147  
 Moore B., Ghigna S., Governato F., Lake G., Quinn T., Stadel J., Tozzi P. 1999b, *ApJ*, 524, 19L  
 Navarro J. F., Frenk C. S., White S. D. M. 1996, *ApJ*, 462, 563  
 Navarro J. F., Frenk C. S., White S. D. M. 1997, *ApJ*, 490, 493  
 Nakamura T. K. 2000, *ApJ*, 531, 739  
 Pearce F. P., Thomas P. A., Couchman H. M. P. 1993, *MNRAS*, 264, 497  
 Power C., Navarro J. F., Jenkins A., Frenk C. S., White S. D. M., Springel V., Stadel J., Quinn T. 2003, *MNRAS*, 338, 14  
 Quinlan G. D. 1996, *New Astronomy*, 1, 255

- Salucci P. 2001, MNRAS, 320, L1  
Simon J. D., Bolatto A. D., Leroy A. L., Blitz L. 2003, ApJ, 596, 957  
Spergel D. N., Hernquist L. 1992, ApJ, 397, L75  
Springel V., Yoshida N., White S. D. M. 2001, New Astronomy, 6, 79  
Swaters R. A., Madore B. F., van den Bosch F. C., Balcells M. 2003, ApJ, 583, 732  
Taffoni G., Mayer L., Colpi M., Governato F. 2003, MNRAS, 341, 434  
Taylor J. E., Babul A. 2001, ApJ, 389, 5  
Taylor J. E., Navarro J. F. 2001, ApJ, 563, 483  
Toomre A., Toomre J. 1972, ApJ, 178, 623  
Velázquez H., White S. D. M. 1999, MNRAS, 304, 254  
White S. D. M. 1978, MNRAS, 184, 185  
White S. D. M. 1979, MNRAS, 189, 831  
White S. D. M., Rees M. 1978, MNRAS, 183, 341  
Widrow L. M. 2000, ApJS, 131, 39